Chaotic tracer dynamics in open hydrodynamical flows†

By G. KÁROLYI[1], Á. PÉNTEK[2], T. TÉL[3] AND Z. TOROCZKAI[4]

[1]Research Group for Computational Mechanics of the Hungarian Academy of Sciences, Budapest, Hungary

[2]Institute for Pure and Applied Physical Sciences, University of California, San Diego, La Jolla, USA

[3]Institute for Theoretical Physics, Eötvös University, Budapest, Hungary

[4] Virginia Polytechnic Institute and State University, Blacksburg, USA

We investigate the dynamics of tracer particles in time-dependent open flows. In cases when the time-dependence is restricted to a finite region, we show that the tracer dynamics is typically chaotic but necessarily of transient type. The complex behaviour is then due to an underlying nonattracting chaotic set that is also restricted to a finite domain, and the tracer dynamics corresponds to a kind of chaotic scattering process. Examples are taken from the realm of two-dimensional incompressible flows. The cases of two leapfrogging vortex pairs and of the blinking vortex–sink system illustrate the phenomenon in inviscid fluids, while the von Kármán vortex street problem belongs to the class of viscous flows. Based on these examples, generic features of the scattering tracer dynamics are summarized.

1. Introduction

The advection of particles in hydrodynamical flows is a phenomenon having attracted great recent interest from the side of dynamical system community because these particles can exhibit chaotic motion, see Aref & Balachandar (1986) and Péntek *et al.* (1995b). By particle we mean a light granule of small extension. If it takes on the velocity of the flow very rapidly, i.e. inertial effects are negligible, we call the advection passive, and the particle a passive tracer. Its equation of motion is then

$$\dot{\mathbf{r}} = \mathbf{v}(\mathbf{r}, t), \tag{1.1}$$

where $\mathbf{v}$ represents the velocity field that is assumed to be known. The tracer dynamics is thus governed by a set of ordinary differential equations, like e.g. for driven anharmonic oscillators, whose solution is typically chaotic.

It is a unique feature of chaotic advection in time-dependent *planar incompressible* flows that the fractal structures characterizing chaos in phase space become observable by the naked eye in the form of spatial patterns. In such cases there exists a *stream function* ψ, see Milne-Thomson (1958) and Landau & Lifshitz (1959), whose derivatives can be identified with the velocity components as

$$v_x(x, y, t) = \frac{\partial \psi}{\partial y}, \quad v_y(x, y, t) = -\frac{\partial \psi}{\partial x}, \tag{1.2}$$

and whose level lines provide the streamlines. Note that (1.2) is a consequence of incompressibility because it implies $\nabla \mathbf{v} = 0$. Combining this with (1.1) for a planar flow where $\mathbf{r} = (x, y)$ and $\mathbf{v} = (v_x, v_y)$, one notices that the equations of motion have canonical character with $\psi(x, y, t)$ playing the role of the Hamiltonian and x and y being the

† This paper is dedicated to Professor K. Nagy on the occasion of his 70th birthday.

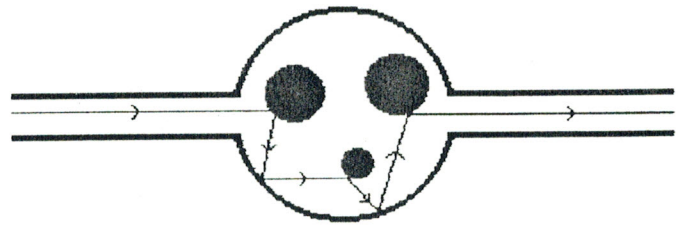

FIGURE 1. Schematic diagram representing the dynamics as chaotic scattering in a system defined by two channels and a scattering region containing billiard scatterers.

canonical coordinates and momenta (or *vice versa*), respectively. Thus, the plane of the flow *coincides* with the particles' phase space. This property makes passive advection in planar incompressible flows especially appealing and a good candidate for an experimental observation of patterns that are hidden otherwise in the abstract phase space. In stationary flows, where ψ is independent of t, problem (1.1), (1.2) is integrable and the particle trajectories coincide with the streamlines. In time-dependent cases, however, particle trajectories and streamlines are different, and the former ones can only be obtained by solving equations (1.1), (1.2).

Here we consider passive advection in *open* flows in cases when complicated tracer movements caused by the time-dependent flow is assumed to be restricted to a *finite* region. This will be called the *mixing region* outside of which the time-dependence of ψ is negligible. It is worth emphasizing that a complicated flow field (turbulence) inside the mixing region is not at all required for complex tracer dynamics and the corresponding fractal patterns. Even simple form of time dependence, e.g. a periodic repetition of the velocity field is sufficient.

For tracers injected into the flow outside of the mixing region, where the flow is still practically stationary, the motion is initially simple and becomes later gradually more complicated as the particle is being advected into the mixing region. The advection dynamics can thus be regarded as a *scattering process*, with the advected particles being 'scattered' on the finite region of nontrivial mixing. The motion in the outflow region is then simple again. Thus, for such processes chaos is necessarily restricted to a finite region both in space and time. We claim that this *transient chaos*, Tél (1990), is the only form of chaos which can appear in the situation studied. Tracer dynamics then corresponds to a kind of *chaotic scattering*, see Smilansky (1992), which is a subfield of nonlinear dynamics with a considerable amount of accumulated knowledge. The interpretation of certain advection phenomena, observable also in experiments, is thus very natural in this framework.

Symbolically, we can indentify the tracer dynamics in the inflow and outflow region with the motion of a point mass in a channel in front of and after a scattering region, respectively. The scattering region characterized either by strongly varying forces or, in billiards, by the presence of scatterers corresponds then to the mixing region in the advection problem (see figure 1). Tracer particles are thus topologically similar to point mass trajectories in a scattering system. We have to bear in mind, however, that the analogy is not complete since the point mass problem's phase space is four-dimensional.

The complicated form of trajectories implies a long time spent in the mixing region. In other words, tracers can be temporarily trapped there. Due to the incompressibility of the flow no attractors can exist, and *almost all* particles escape the mixing region. This *escaping* property is a specific characteristic of chaotic scattering and of the tracer dynamics in open flows of the type we are studying. As a consequence, the underlying

chaotic set is a *chaotic saddle* with more pronounced fractal character than chaotic attractors, since the former has a Cantor set type structure along *both* the unstable and the stable direction. Instead of following a deductive approach, in the next section we study examples where the time dependence is the simplest possible one, periodic. Without giving mathematical details, we just introduce the problems and pictorially show the flow fields, some typical tracer trajectories, and the invariant sets obtained in numerical simulations. The generic features are then summarized and discussed in the last, concluding section.

2. Case studies

2.1. *Leapfrogging vortex pairs*

We consider a model of the so-called 'leapfrogging' motion of two smoke rings, see Beigie *et al.* (1994), Van Dyke (1982), Shariff *et al.* (1988), Shariff & Leonard (1992) and Saffman (1992). If the rings have the same sense of rotation and move along the same axis, the rear vortex ring attempts to pass through the front one. The leading ring then widens due to the mutual interaction and slows down. Simultaneously, the other ring shrinks, accelerates and penetrates the first one. This process is then repeated continuously with some period. We studied, Péntek *et al.* (1995a), the two-dimensional analogue of this process: advection in the field of two pairs of ideal point vortices of the same strength and moving along the same symmetry axis (the x-axis) which also exhibit a strictly periodic motion. The equations of motion for the vortices can easily be written down by using the rules of point vortex interactions, Saffman (1992), and can numerically be solved with high accuracy, see Péntek *et al.* (1995a).

Figure 2 exhibits the streamline pattern at two different instants of time, at $t = 0$ and $t = T/2$ in a frame co-moving with the center of mass of the vortex pairs, where T denotes the period of the velocity field. Since the vortex pairs are identical, this period is half of the leapfrogging motion's period. Note the smoothness of the streamlines. The tracer motion in any frozen-in streamline pattern would be simple, it is the temporal variation of ψ that leads to irregular motion.

The stream function $\psi(x, y, t)$ is analytically known, and tracer trajectories can be obtained by solving equations (1.1), (1.2) with this time dependent stream function as an input, see Péntek *et al.* (1995a). Figure 3 contains, in the same co-moving frame, the plot of two complicated, chaotic scattering trajectories of tracers injected into the flow in front of the vortex pairs. The drastical difference in the shape of the trajectories due to a slight change in the initial y coordinates is an example for the sensitive dependence on the initial conditions, which is regarded as a common manifestation of chaos. A comparison with figure 1 shows that the channels towards and away from the scattering region correspond to the regions far away in front of and after the vortex pairs, respectively.

Figure 4 presents the invariant sets associated with the scattering tracer dynamics on a stroboscopic map taken at integer multiples of the period T. The time instant selected is $t = 0 \,(\mathrm{mod}\ T)$. The chaotic saddle (see figure 4(a)) is the union of all unstable bounded trajectories trapped in the mixing region forever. It clearly contains parts that appear to be the direct products of two Cantor sets, e.g. the one around the midpoint between the vortices. Such parts form the *hyperbolic* component of the saddle. There are also rather densely occupied regions forming the *nonhyperbolic* component, situated around curves surrounding the vortices. Note the white regions around the vortices that are not accessible by tracers coming from outside. Thus, in spite of the infinitesimally small extension of the vortices in the Eulerian velocity field, finite vortex 'cores' are formed

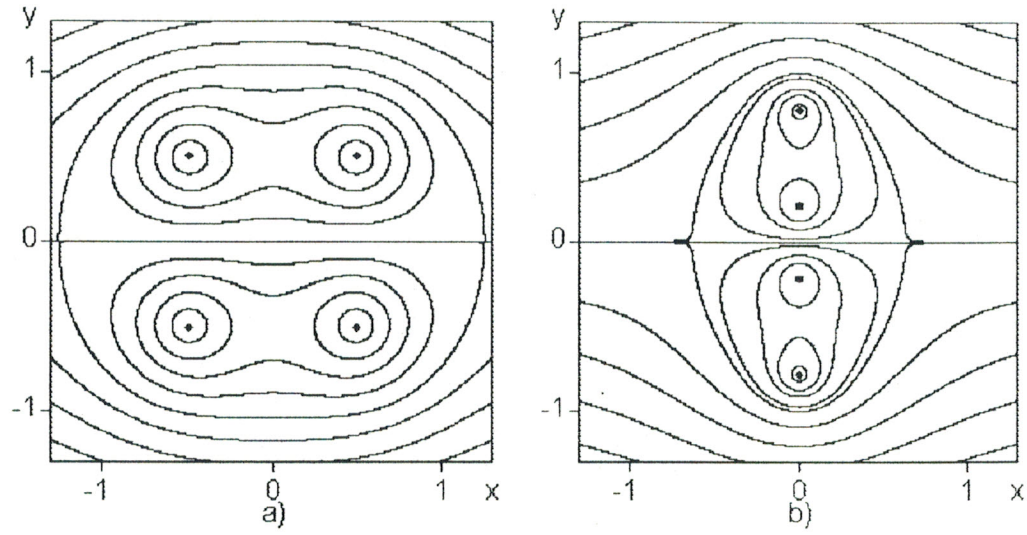

FIGURE 2. Streamlines of the leapfrogging vortex pair problem at (a) $t = 0$ and (b) $t = T/2$. The vortices in the upper (lower) half plane have the same strength, 1 (-1) in dimensionless units. The initial condition $(t = 0)$ is a configuration where the width of both vortex pairs as well as their distance along the x-axis is unity. The vortex centers are denoted by black dots.

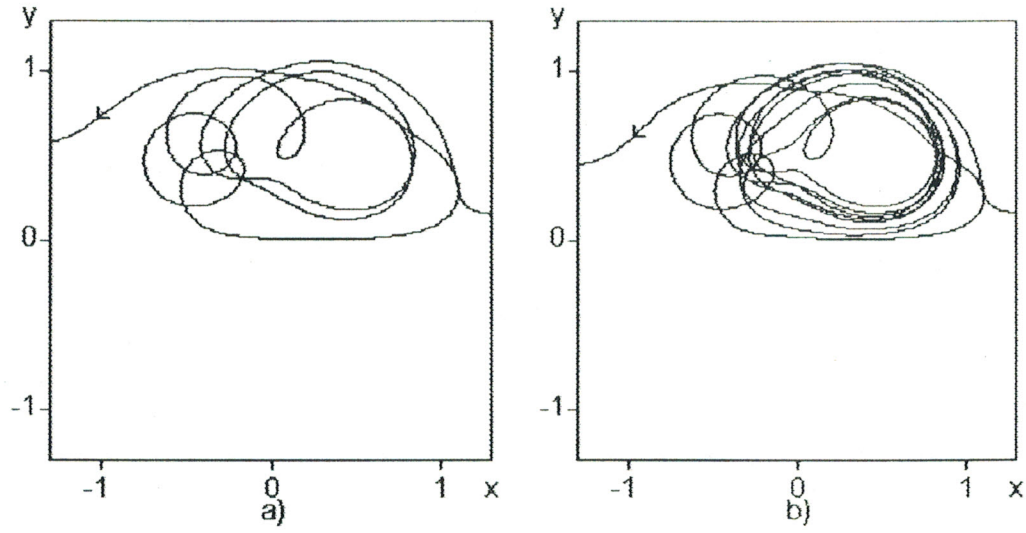

FIGURE 3. Two complicated tracer trajectories with initial y coordinates differing by 10^{-2} in the leapfrogging problem presented in a frame co-moving with the vortex pairs' center of mass.

in the tracer dynamics. The boundaries of the vortex cores are, in the language of dynamical system theory, KAM tori, see Wiggins (1992). The nonhyperbolic component of the saddle surrounds these tori.

Other invariant sets are the stable and unstable manifolds of the chaotic saddle. The stable manifold is the set of initial conditions for tracers that reach the chaotic saddle asymptotically. Since the latter is not an attractor, the stable manifold must be a set of measure zero, i.e. a set whose area is vanishing. It is thus a fractal whose form is given in figure 4(b) at the same instant of time as the saddle of figure 4(a). The unstable manifold (see figure 4(c)) is traced out by trajectories that have approached the saddle with rather high accuracy and left it after staying in its vicinity for a long time. In this

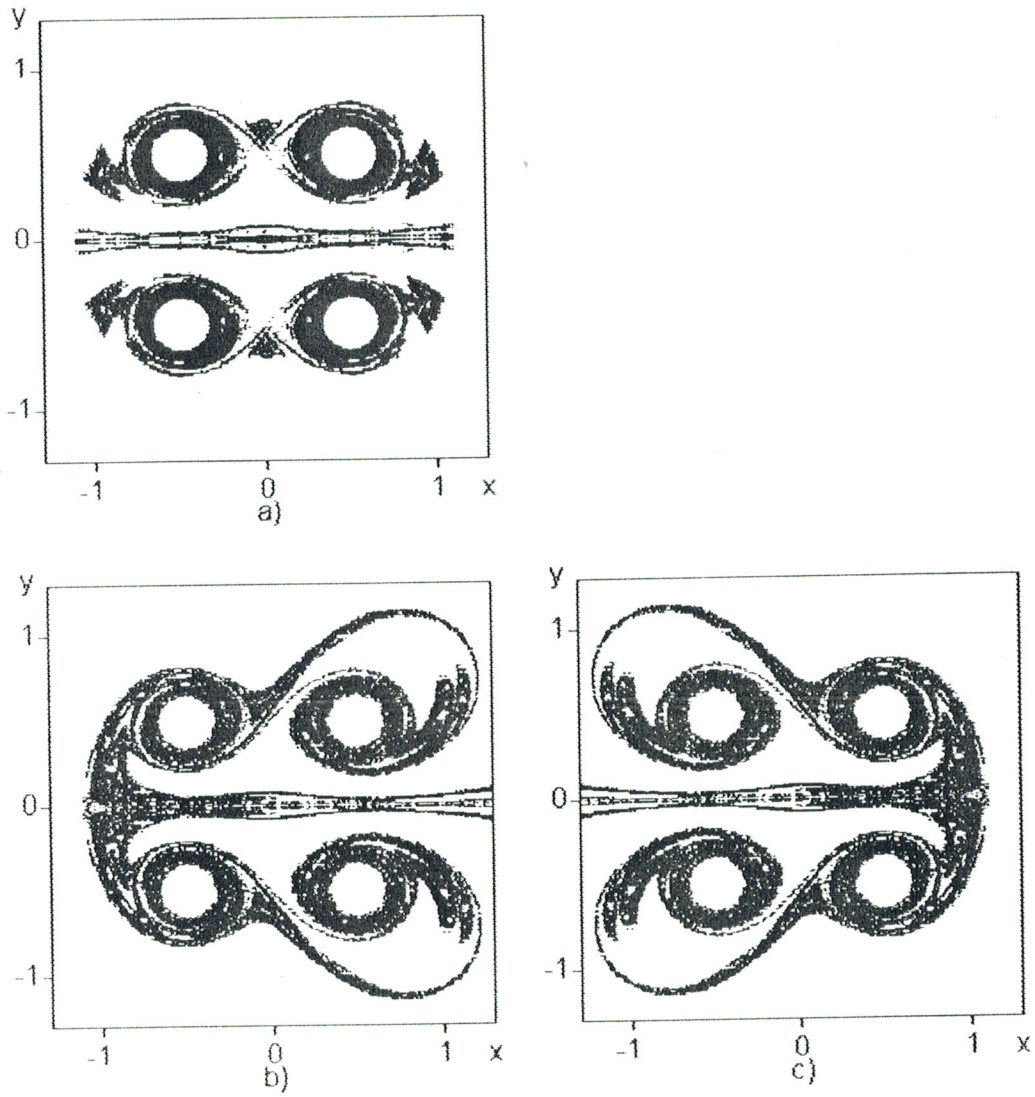

FIGURE 4. Stroboscopic section of the invariant sets of the leapfrogging vortex pairs at $t = 0 \pmod{T}$: (a) Chaotic saddle, (b) stable manifold, (c) unstable manifold.

particular example and at this time instant, this manifold turns out to be the mirror image of the stable manifold with respect to the y axis.

2.2. *The blinking vortex–sink system*

Consider an ideal fluid filling in the infinite plane with a point vortex that is simultaneously sinking. This can be a model of a large bath tub with a sink since a rotational flow is formed around the sink in the course of the outflow. The blinking vortex–sink system introduced originally by Aref *et al.* (1989) is obtained by having two such sinking vortex points some distant apart from each other and being active alternatingly for a duration of $T/2$. This models the outflow from a large bath tub with two sinks that are opened in an alternating manner. In the blinking vortex–sink system the velocity field is periodic with T but in a special way: it is stationary for a half period of $T/2$ and stationary again but of another type for the next half period of $T/2$.

By using the complex function formalism, Milne-Thomson (1958), for describing these stationary flows, one can write down the stream functions explicitly. The streamlines valid for $0 < t \leq T/2$ and $T/2 < t \leq T$ are shown in figures $5(a)$ and $5(b)$, respectively.

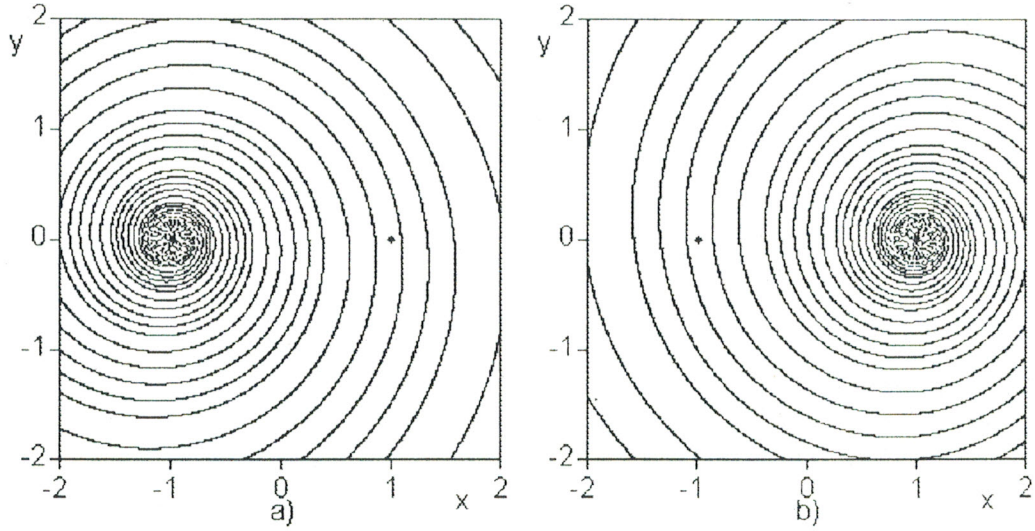

FIGURE 5. Streamlines of the blinking vortex–sink system for (a) $0 < t \leq T/2$ and (b) $T/2 < t \leq T$. The two vortex–sink centers are situated at $x = \pm 1$ in dimensionless units.

Note that sufficiently far away from the origin the differences between the streamlines and the stream functions of the two cases are negligible. Since the time-dependence appears in the form of a jump of ψ at $t = 0 \,(\mathrm{mod}\ T/2)$, the tracer dynamics is analogue to that of a kicked mechanical system. The replacement of a tracer particle can easily be determined within any of the stationary regimes. The comparison of the particles' position right after the first flow field sets in, i.e. at $t = 0^+ \,(\mathrm{mod}\ T)$, leads to a stroboscopic map whose form can be given analytically, see Aref *et al.* (1989). The tracer dynamics is governed in this system by a discrete dynamics rather than by a differential equation and is thus simpler to study. Both sinks are surrounded by a circle of a given radius containing all the points that escape the system within a duration of $T/2$. These two disks correspond to the channel directing particles away from the scattering region of figure 1, while the motion far away from the sinks corresponds to that inside the channel leading towards the scatterers.

The advection problem has two essential dimensionless parameters: the sink strength and the ratio of the vortex and sink strengths. We have carried out a detailed investigation of the tracer dynamics at different values of the parameters, see Károlyi (1995). Two tracer trajectories are shown in figure 6 with long life time before reaching one of the sinks. The breakpoints are due to the sudden jumps between the two different streamline patterns at $t = 0 \,(\mathrm{mod}\ T/2)$.

The invariant sets characterizing this problem are shown in figure 7 on a stroboscopic map taken at time $t = 0^+ \,(\mathrm{mod}\ T)$. The chaotic saddle (see figure $7(a)$) seems to be hyperbolic everywhere, i.e. to have a direct product structure. At other ratios of the sink and vortex strengths KAM tori might also appear and in their vicinity the chaotic saddle is nonhyperbolic. The invariant manifolds are given in figures $7(b)$ and $7(c)$. The stable manifold (see figure $7(b)$) is a fractal curve reaching arbitrarily far away from the vortex–sink centers. Its form is more and more regular when going out to infinity due to the simplicity of the flow in this region. In contrast, the unstable manifold (see figure $7(c)$) is a fractal curve bounded to a finite region and connects the chaotic saddle with the right sink closed at $t = 0^- \,(\mathrm{mod}\ T)$, just before taking the stroboscopic map.

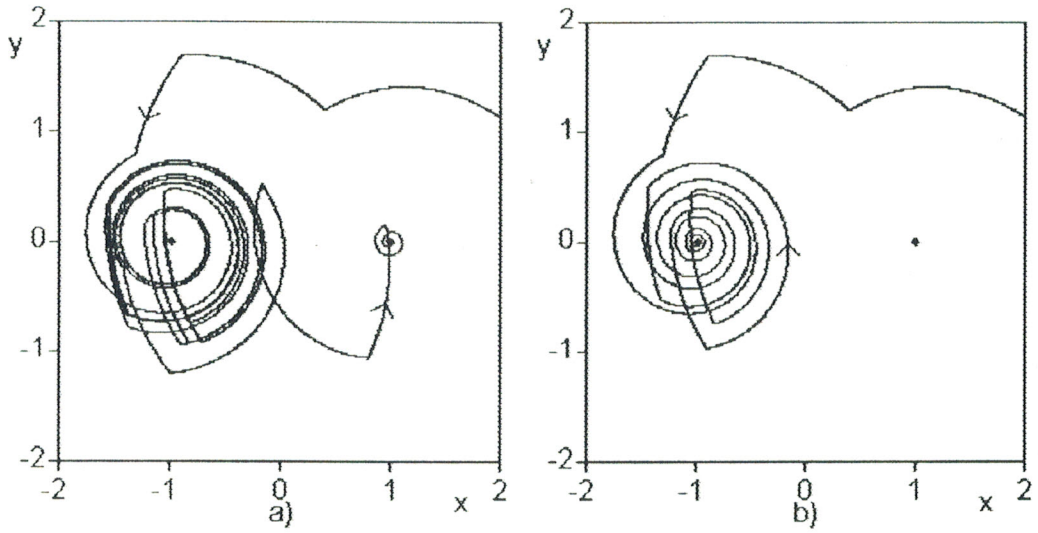

FIGURE 6. Two complicated tracer trajectories of the blinking vortex–sink system. A change of 10^{-2} in the initial coordinates leads to completely different trajectories leaving the system through different sinks. The vortex–sink centers are denoted by black dots.

2.3. *The von Kármán vortex street*

We consider the flow of a viscous fluid around a cylinder with a background velocity pointing along the x-axis. At intermediate background velocities (whose dimensionless measure, the Reynolds number, is on the order of 10^2) no stationary velocity field is stable, instead, a strictly periodic behaviour sets in with period T. Two vortices are created behind the cylinder within each period, one above and the other one below the x-axis. These two vortices are delayed by a time $T/2$. Note that they are now extended vortices with finite velocities even in the vortex centers. The vortices first grow in size, then become detached from the cylinder and start to drift along the channel. This alternating separation of vortices from the upper and lower cylinder surface is called the von Kármán vortex street and is characterized by a strictly periodic velocity field of period T, see Van Dyke (1982) and Beigie *et al.* (1994). After a short length of travel, the vortices are destabilised and destructed due to the viscosity of the fluid. Far away from the cylinder upstream and downstream the flow is, however, practically stationary.

To obtain the velocity distribution one has to solve the two-dimensional inviscid Navier-Stokes equations with no-slip boundary condition along a circle, see Shariff *et al.* (1991) and Jung & Ziemniak (1992). For simplicity we use here an analytic model for the stream function introduced in Jung *et al.* (1993). It was motivated by a direct numerical simulation of the Navier–Stokes flow carried out by Jung & Ziemniak (1992) at Reynolds number 250.

Figures 8(a) and 8(b) show the streamlines of this model at time $t = 0 \,(\mathrm{mod}\ T)$ and $t = T/4 \pmod{T}$. The streamlines far away from the cylinder are straight at any instant of time. Thus, the channels towards and away from the scattering region of figure 1 correspond in this case to the upstream and downstream regions, respectively. Tracer trajectories were generated, see Jung *et al.* (1993), Ziemniak *et al.* (1994), Péntek *et al.* (1995b), by solving equations (1.1), (1.2) with the model stream function of Jung *et al.* (1993). Figure 9 exhibits two complicated scattering trajectories that are trapped for a while in the wake of the cylinder.

The invariant sets are shown again on a stroboscopic map taken at integer multiples of the period T in an area surrounding the cylinder. The chaotic saddle (see figure 10(a))

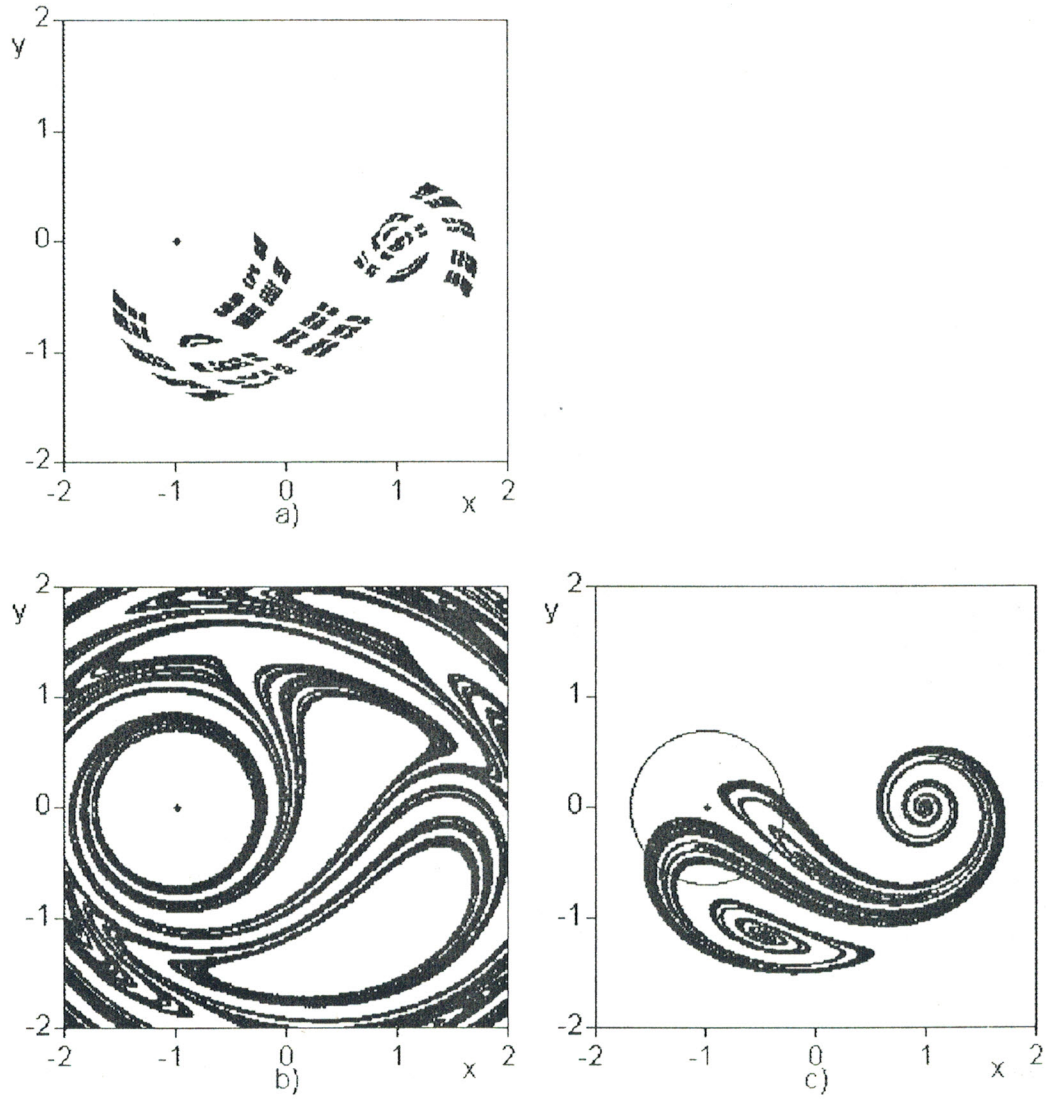

FIGURE 7. Stroboscopic section of the invariant sets of the blinking vortex–sink system at $t = 0^+ \pmod{T}$: (a) Chaotic saddle, (b) stable manifold, (c) unstable manifold. The circle around the left vortex–sink center at $(-1, 0)$ indicates the area from which the tracers leave the system via the left sink during the first half period.

contains now both a hyperbolic and a nonhyperbolic component. The former one is situated away from the cylinder, while the nonhyperbolic component seems to accumulate on the cylinder's surface. This is a nice manifestation of the no-slip boundary condition. Very close the the surface, i.e. in the boundary layer, the velocity must be small and there can exist therefore increasingly many trapped trajectories. In fact, the surface contains an infinity of parabolic orbits, see Jung *et al.* (1993), and it plays a similar role as a KAM surface. This surface is, however, smooth and does not have surrounding cantori. Nevertheless, the effect of both types of tori is similar in collecting the nonhyperbolic component of the chaotic saddle.

The invariant manifolds are exhibited in figures $10(b)$ and $10(c)$. The stable manifold (see figure $10(b)$) surrounds the cylinder surface and extends to the infinitely far inflow region in a narrow band close to the negative x-axis. In contrast, the unstable manifold (see figure $10(c)$) touches the cylinder surface along a finite arch only, and extends to the outflow region at infinity in a strongly oscillating way. It is interesting to note, that

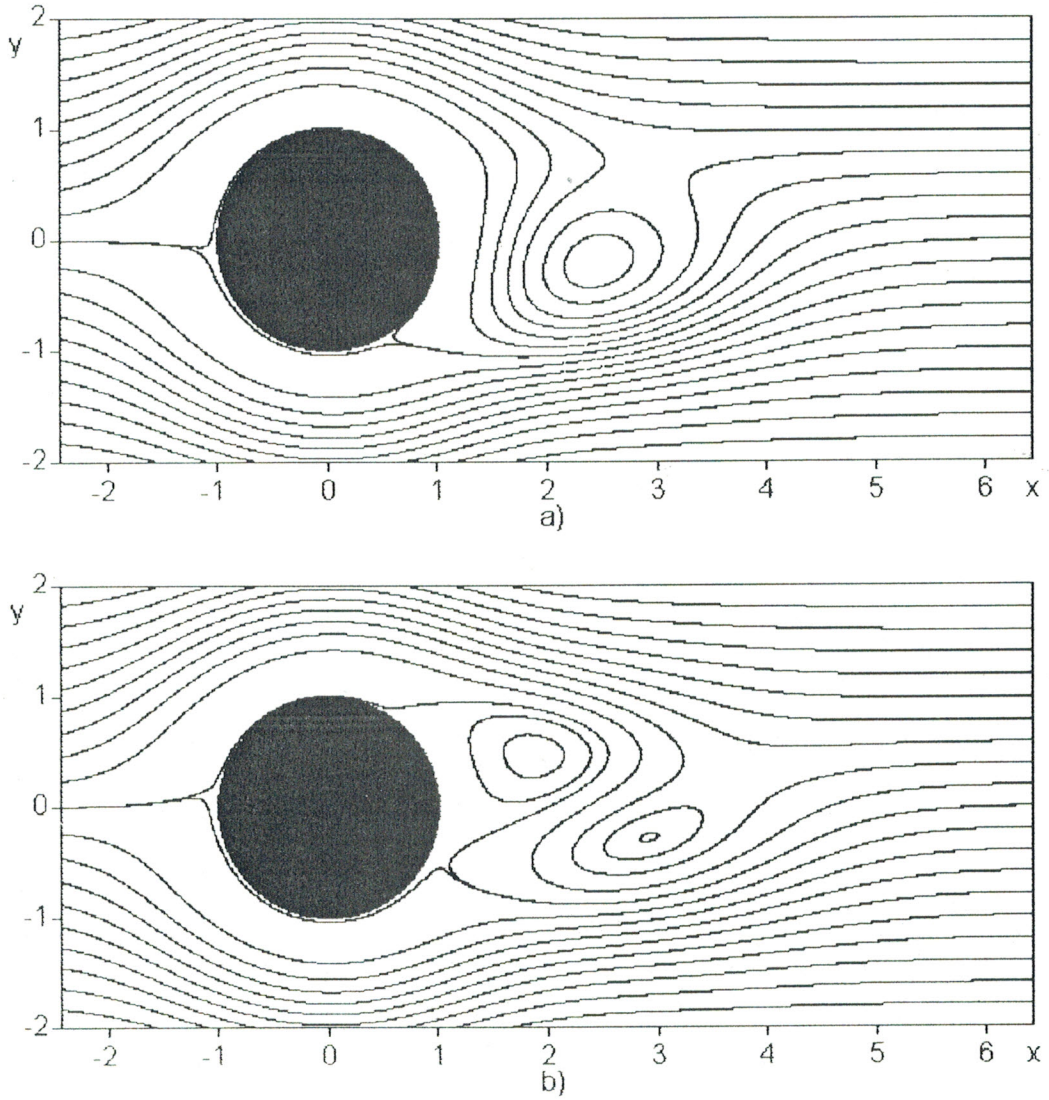

FIGURE 8. Streamlines of the von Kármán vortex street flow at (a) $t = 0$ and (b) $t = T/4$, obtained by using the form and parameters of the model of Jung *et al.* (1993). The radius of the cylinder is 1 in dimensionless units and its center is in the origin. Due to a symmetry of the flow, the streamline pattern at time $t = T/2\,(\mathrm{mod}\ T)$ and $t = 3T/4\,(\mathrm{mod}\ T)$ can be obtained as the mirror images of (a) and (b), respectively.

in this system a small chaotic saddle is formed around $x = 3$ downflow, too, with its own invariant manifolds, see Péntek *et al.* (1995b). This saddle is fully hyperbolic and rather unstable, therefore, its dynamical consequences are not so apparent as the ones discussed above and shown in figure $10(a)$.

3. Conclusions

Based on the examples, we summarize the most important general features characterizing chaotic passive advection in open flows of the type investigated.

• *The existence of a chaotic saddle* is the key observation in understanding the scattering tracer dynamics. This set, just like a chaotic attractor, is the union of all *bounded orbits*, including periodic ones, never escaping the mixing region. These orbits are all unstable. In contrast to a chaotic attractor, however, the chaotic saddle has practically no

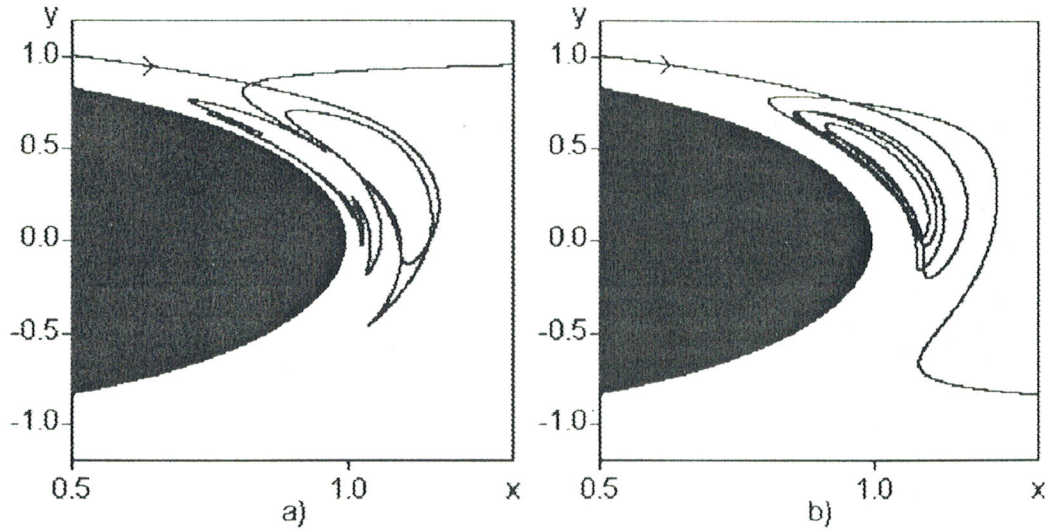

FIGURE 9. Two complicated tracer trajectories in the von Kármán vortex street with initial y coordinates differing by 10^{-2}. The horizontal scale is multiplied by 3 for better visualization.

region of attraction. In other words, the chaotic saddle contains only those orbits which are trapped in the mixing region forever. They are rather exceptional ones and not even their closure covers a finite area of the plane, although they are *infinite* in number. Such orbits form a *fractal subset* of the mixing region.

• *Hyperbolic and nonhyperbolic components* are subsets of the chaotic saddle. The first one contains the strongly unstable trapped orbits with local Lyapunov exponents on the order of unity whose neighbourhood will be left by tracer particles rather rapidly. The nonhyperbolic component is the union of weakly unstable trapped orbits with positive local Lyapunov exponents below a threshold, among which orbits with arbitrarily small positive Lyapunov exponents can also be found. This component lies around KAM tori or other sticky surfaces appearing due to no-slip boundary conditions. The separation of these components is somewhat arbitrary (because the value of the threshold Lyapunov exponent can be freely chosen from the range, say, between 0.1 and 0.01 in dimensionless units) and also geometrically somewhat interwoven. Nevertheless, they are responsible for qualitatively different types of motions (see below) and this is why their distinction is rather useful.

• *The stable manifold* is a complicatedly winding curve along which the chaotic saddle can be reached. Tracers with long lifetime can only be the ones approaching the chaotic saddle close along its stable manifold. Thus the stable manifold can also be considered as the 'basin of attraction' of the saddle. It must have a vanishing area because in a Hamiltonian system no attractor can exist. By means of video techniques this manifold can also be determined in an experiment as suggested by Ziemniak *et al.* (1994) and Péntek *et al.* (1995b). Sprinkle tracers in a domain of the flow, record their trajectories, and keep only those whose lifetime in the mixing region is sufficiently long. By plotting the initial points of these trajectories one obtains a good approximant to the stable manifold.

• *The unstable manifold* of the saddle is the set of points along which particles, after entering a close neighbourhood of the set, leave this neighbourhood. This manifold appears on a stroboscopic map as a rather complicatedly winding curve and extends to the region where particles exit the flow. As a consequence, a droplet of particles injected into the flow in front of the mixing region will, after a long time, trace out the

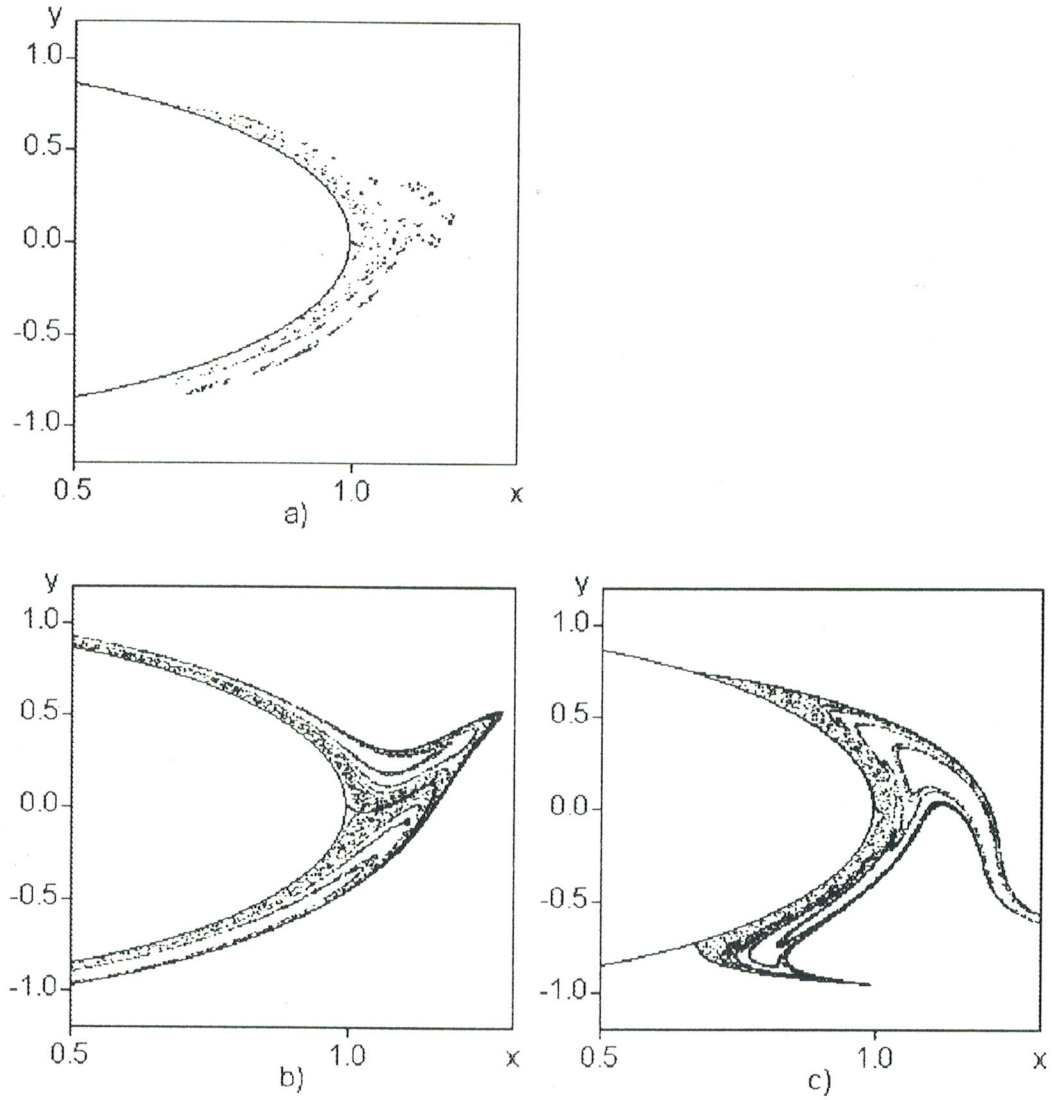

FIGURE 10. Stroboscopic section of the invariant sets in the von Kármán vortex street at $t = 0$ (mod T): (a) Chaotic saddle, (b) stable manifold, (c) unstable manifold. The horizontal scale is multiplied by 3 for better visualization.

unstable manifold, provided the droplet overlaps initially with the stable manifold. This fact makes the unstable manifold a direct physical observable of the passive advection problem, see Ottino (1989) and Beigie *et al.* (1994), and provides the easiest method to plot this manifold experimentally or numerically. (In simulations, the stable manifolds can best be obtained as the unstable ones in the time reversed tracer dynamics. The chaotic saddle is the common part of both invariant manifolds, but there also exist direct powerful methods for its determination, see Nusse & Yorke (1989).)

- *The time delay distribution* is a characteristic of tracer ensembles. Trapped particles have some *time delay* τ relative to the background flow: the longer τ is the more complicated the trajectory becomes. Observe several trajectories (an ensemble) with initial points taken from a closed domain of the flow, or along a straight line. The quantity $P(\tau)d\tau$ is the probability to find a particle with time delay in the interval $(\tau, \tau + d\tau)$. $P(\tau)$ must be a function tending to zero for large times. For intermediate times shorter than some crossover value τ_c it typically decays exponentially,

$$P(\tau) \sim \exp(-\tau/\bar{\tau}). \tag{3.3}$$

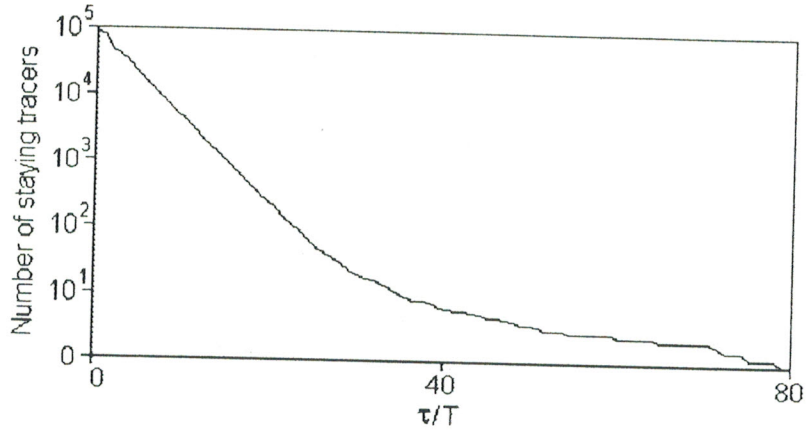

FIGURE 11. A typical time delay distribution $N_0 P(\tau)$ characterizing chaotic tracer dynamics with N_0 as the number of tracer trajectories. For $\tau \ll \tau_c \approx 30T$ and $\tau \gg \tau_c$ equation (3.3) and equation (3.4) holds, respectively. Data are taken from the blinking vortex–sink system with parameter values where KAM tori exist, see Károlyi (1995).

It is only the prefactor, not written out here, that depends on the choice of the initial distribution. For much longer times than the crossover value one observes an algebraic decay

$$P(\tau) \sim \tau^{-\sigma} \tag{3.4}$$

(see figure 11). In periodic flows it is natural to measure τ in units of the velocity field's period, T. We claim that the first behaviour is due to the *hyperbolic* component containing trapped orbits with large local Lyapunov exponents. $\bar{\tau}$ is the average time delay that can then also be considered as the *average lifetime* of chaos on the hyperbolic component and is generally on the order of a few times the flow period. The algebraic decay is a consequence of the presence of neutral trapped orbits, and the exponent σ characterizes the stickiness of the tori. Thus the following qualitative picture emerges concerning the scattering tracer dynamics. Particles starting not exactly on the stable manifold have finite lifetimes in the mixing region. Their motion can be considered as a random walk among the periodic orbits of the chaotic saddle. Those with a not very long lifetime just wander among strictly hyperbolic orbits and have an average lifetime $\bar{\tau}$. The very persistent trajectories must have visited the nonhyperbolic part and their long-time statistics is therefore nonexponential.

- *The time delay function.* A more detailed characterization of the trapping process is based on the observation of individual trajectories. Let us inject tracer particles into the flow along a line and determine the time τ they spend in the mixing region. This defines a function $\tau(y)$ where y denotes the inital position along the line of injection. A unique sign of chaotic tracer scattering is the rather *irregular* appearance of the time delay function as illustrated by figure 12. The intersection of the stable manifold with the line of initial conditions marks points with formally infinite delay times. The different time delays of neighbouring points indicate again the high sensitivity to initial conditions. An irregular scattering function is thus a characteristic of chaotic advection in open flows. The time delay distribution $P(\tau)$ reflects global properties of the scattering process and can easily be derived from the time delay $\tau(y)$ of the trajectories: $P(\tau)\mathrm{d}\tau$ is proportional to the number of tracers whose time delay falls into the interval $(\tau, \tau + \mathrm{d}\tau)$ when integrating over all initial conditions y.
- *Fractal properties of the invariant sets.* First note that the fractal dimension of

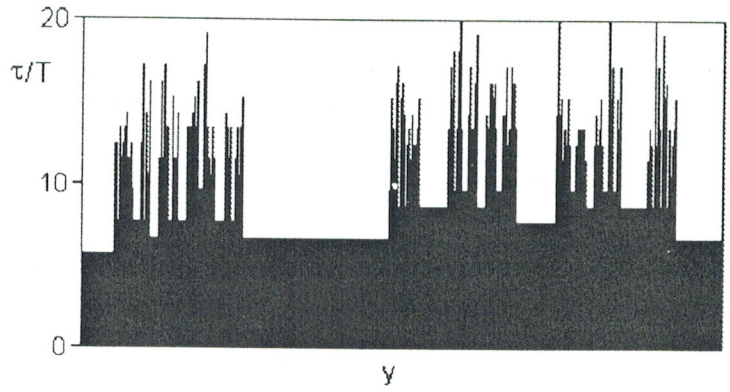

FIGURE 12. A typical irregular time delay function $\tau(y)$ with discrete time delays measured in integer multiples of the flow's period T (data are taken again from the blinking vortex–sink system, see Károlyi (1995)). The large time delay values mark inital conditions with a long trapping in the mixing region. Note the sensitive dependence of τ on y, a criterion for chaotic behaviour.

the Cantor sets whose direct product is the chaotic saddle's hyperbolic component is always a positive number d_0 less than unity. Next, use the fact that the dimension of a direct product of two fractals is the sum of the components' fractal dimensions, see Falconer (1985). Thus, the chaotic saddle's hyperbolic component is of fractal dimension $d_{\text{set}} = 2d_0$. The manifolds emanating from this component are the direct products of a line and a Cantor set, therefore, $d_{\text{manifold}} = 1+d_0$. Note that because of the time reversal symmetry of the canonical equations of motion (1.1), (1.2), the stable and unstable manifolds have common scaling properties and have therefore identical dimensions.

The fractal properties of the nonhyperbolic component are different. In these regions the partial fractal dimension of the chaotic set tends to unity in the limit of extremely fine resolution, see Lau *et al.* (1991). The escape rate and the average Lyapunov exponent are expected to be zero on this component, see Christiansen & Grassberger (1993), in accordance with (3.4). Therefore a fat fractal behaviour becomes evident when increasing the spatial resolution: $d_{\text{set}} \to 2$ and $d_{\text{manifold}} \to 2$. In numerical simulations it might be hard to reach the resolution where the fat fractal property of the manifolds is evident away from the immediate vicinity of the nonhyperbolic component. Thus, we can state that on the practically relevant length scale of 10^{-4} or larger (in dimensionless units) the tracer patterns appear as real fractals with noninteger dimensions.

- *Singularities of the time delay function* sit in points where the line of initial conditions intersect the stable manifold. Thus, with a resolution larger than some critical value ϵ_c, the dimension of singularities is the same value as that of the component Cantor sets: $d_{\text{sing}} = d_0$. On finer scales, one observes a crossover to a fat fractal behaviour and $d_{\text{sing}} \to 1$. The critical resolution ϵ_c, just like the crossover time τ_c, might depend on the position of the line of initial conditions.

- *Fractal tracer boundaries* are easy to generate in open time-periodic flows. One way is to inject dye particles continuously into the flow along a line so that the colours are different in two neighbouring segments, see Péntek *et al.* (1995b), and investigate how the boundary evolves in time. Alternatively, one can also divide the fluid in strips of different colours and study the deformation of the boundaries, see Péntek *et al.* (1995a). After a long time of observation, the boundaries become rather complex containing a fractal part that is nothing but the *unstable* manifold of the chaotic saddle, see Péntek *et al.* (1995b). A different type of boundary is obtained by clouring the inital points according to how

the tracers exit the mixing region. In a problem like the blinking vortex–sink system, the most natural choice is to use different colours for exiting via different sinks, see Aref *et al.* (1989). More generally, one can colour the initial points depending on whether the trajectories cross a preselected line outside of the mixing region in a given segment or not. The fractal part of such boundaries will contain the *stable* manifold of the chaotic saddle, see Péntek *et al.* (1995b). The second type of boundary is an extension of the fractal basin boundary concept, see Grebogi *et al.* (1983), for Hamiltonian systems without any attractors. For both types of boundaries their fractal dimension is the same as that of the manifolds: $d_{\text{boundary}} = d_{\text{manifold}} = 1 + d_0$.

• *Relation between dynamical and fractal properties.* Chaotic advection in open flows is a phenomenon where one clearly sees how the underlying dynamics determines the fractal properties of the chaotic set and its manifolds. Due to a general relation valid for any kind of transient chaos, see Kantz & Grassberger (1985) and Tél (1990), the fractal dimension d_0 of a component Cantor set appears as

$$d_0 \approx 1 - \frac{1}{\bar{\lambda}\bar{\tau}}, \tag{3.5}$$

where $\bar{\lambda}$ is the (positive) average Lyapunov exponent of trajectories spending a long time around the chaotic saddle. This formula says that the deviation of the fractal dimension from unity is proportional to the ratio of two average times characterizing local and global instability. The quantity $1/\bar{\lambda}$ is the average time of the separation of nearby trajectories by a factor of e, while $\bar{\tau}$ is the characteristic time, defined by (3.3), of emptying a given area. Between two sets with the same Lyapunov exponent, the one with larger average chaotic lifetime has the larger dimension.

• *More general flows.* Finally we note that the features summarized here seem to be robust. A weak deviation from the flow's planar character makes the canonical form unvalid for the tracer dynamics, nevertheless, a chaotic saddle will govern the process in the three-dimensional phase space of (1.1). Similarly, if the particles have inertia, the dimension of the phase space doubles due to the appearance of physical momenta, even in the crudest approximation. In the simplest case of a planar flow, the phase space is four dimensional in which a chaotic saddle exists. What we observe as tracer patterns is then related to the projection of the invariant manifolds to the plane of the flow. Furthermore, if the flow is slightly compressible, a large number of periodic attractors are expected to appear in the tracer dynamics. They can thus only have rather tiny basins of attractions. Consequently, the dynamics is dominated by the extended chaotic saddle(s) existing among the attractors producing long average chaotic lifetimes.

We are grateful to Celso Grebogi and Jim Yorke for a most enjoyable and fruitful collaboration. Helpful discussions with them, with J. Kadtke, Z. Kovács, Z. Neufeld, K. G. Szabó and A. Provenzale are acknowledged. This work was partially supported by the Hungarian Science Foundation under grants OTKA T019483, T17493, F17166, and the U.S.–Hungarian Science and Technology Joint Fund under projects JF number 286 and 501.

REFERENCES

Aref, H. & Balachandar, S. 1986 *Phys. Fluids* **29**, 3515.

Aref, H., Jones, S. W., Mofina, S. & Zawadski, I. 1989 *Physica* D **37**, 423.

Beigie, D., Leonard, A. & Wiggins, S. 1994 *Chaos Sol. Fract.* **4**, 749.

Christiansen, F.& Grassberger, P. 1993 *Phys. Lett.* A **181**, 47.

FALCONER, K. 1985 *The Geometry of Fractal Sets.* Cambridge Univ. Press.

GREBOGI, C., *et al.* 1983 *Phys. Lett.* A **99**, 415; see also 1987 *Physica* D **25**, 347.

JUNG, C., TÉL, T. & ZIEMNIAK, E. 1993 *Chaos* **3**, 555.

JUNG, C. & ZIEMNIAK, E. 1992 *J. Phys.* A **25**, 3929; see also ZIEMNIAK, E. & JUNG, C. 1995 *Phys. Lett.* A **202**, 263.

JUNG, C. & ZIEMNIAK, E. 1994 In *Fractals in the Natural and Applied Sciences* (ed. M. M. Novak). North Holland.

KANTZ, H. & GRASSBERGER, P. 1985 *Physica* D **17**, 75.

KÁROLYI, G. 1995 *Diploma work.* In Hungarian; see also KÁROLYI, G. & TÉL, T. To be published.

LANDAU, L. D. & LIFSHITZ, E. M. 1959 *Fluid Mechanics.* Pergamon.

LAU, Y. T., FINN, J. M. & OTT, E. 1991 *Phys. Rev. Lett.* **66**, 978.

MILNE-THOMSON, L. M. 1958 *Theoretical Aerodynamics.* Macmillan.

NUSSE, H. E. & YORKE, J. 1989 *Physica* D **36**, 137.

OTTINO, J. M. 1989 *The Kinematics of Mixing: Stretching, Chaos and Transport.* Cambridge University Press; see also OTTINO, J. M. 1990 *Ann. Rev. Fluid Mech.***22**, 207.

PÉNTEK, Á., TÉL, T. & TOROCZKAI, Z. 1995a *J. Phys.* A **28**, 2191; see also 1995 *Fractals* **3**, 33.

PÉNTEK, Á., TOROCZKAI, Z., TÉL, T., GREBOGI, C. & YORKE, J. A. 1995b *Phys. Rev.* E **51**, 4076.

SAFFMAN, P. G. 1992 *Vortex Dynamics.* Cambridge Univ. Press; see also AREF, H. 1983 *Ann. Rev. Fluid Mech.* **15**, 345; MELESHKO, V. V., *et al.* 1992 *Phys. Fluids* A **4**, 2779; MELESHKO, V. V. & VAN HEIJST, G. J. F. 1994 *Chaos Sol. Fract.* **4**, 977.

SHARIFF, K., LEONARD, A. 1992 *Ann. Rev. Fluid. Mech.* **24**, 235.

SHARIFF, K., LEONARD, A., ZABUSKY N. J. & FERZIGER, J. H. 1988 *Fluid. Dyn. Res.* **3**, 337.

SHARIFF, K., PULLIAM, T. H. & OTTINO, J. M. 1991 *Lect. Appl. Math.* **28**, 613.

SMILANSKY, U. 1992 In *Chaos and Quantum Physics* (ed. M. J. Giannoni *et al.*). Elsevier; see also JUNG, C. 1992 *Acta Phys. Pol.* **23**, 323; OTT, E. & TÉL, T. 1993 *Chaos* **3**, 417; KOVÁCS, Z. & WIESENFELD, L. 1995 *Phys. Rev.* E **51**, 5476.

TÉL, T. 1990 In *Directions in Chaos* (ed. Hao Bai-Lin), vol. 3, pp. 149–221. World Scientific.

VAN DYKE, M. 1982 *An Album of Fluid Motion.* The Parabolic Press.

WIGGINS, S. 1992 *Chaotic Transport in Dynamical Systems.* Springer.

ZIEMNIAK, E., JUNG, C. & TÉL, T. 1994 *Physica* D **76**, 123.